# Final Report

for the Grant Award Entitled by

**"Design of Tunable, Thin, and Wide-band Microwave Absorbers"**

**(Grant No.: FA2386-10-1-4061)**

Submitted to

**Dr. Gregg Jessen**
AOARD
7-23-17, ROPPONGI, MINATO-KU
TOKYO 106-0032

by

**Zhongxiang Shen**
School of Electrical and Electronic Engineering
Nanyang Technological University
50 Nanyang Avenue, Singapore 639798

July 28, 2011

# Report Documentation Page

*Form Approved*
*OMB No. 0704-0188*



| 1. REPORT DATE | 2. REPORT TYPE | 3. DATES COVERED |
|---|---|---|
| **12 AUG 2011** | | |

| 4. TITLE AND SUBTITLE | 5a. CONTRACT NUMBER |
|---|---|
| **Design of Tunable, Thin, and Wide-band Microwave Absorbers** | 5b. GRANT NUMBER |
| | 5c. PROGRAM ELEMENT NUMBER |
| 6. AUTHOR(S) | 5d. PROJECT NUMBER |
| **Zhongxiang Shen** | 5e. TASK NUMBER |
| | 5f. WORK UNIT NUMBER |
| 7. PERFORMING ORGANIZATION NAME(S) AND ADDRESS(ES) | 8. PERFORMING ORGANIZATION REPORT NUMBER |
| **Nanyang Technological University,50 Nanyang Avenue,Singapore 639798,Singapore,NA,NA** | **N/A** |
| 9. SPONSORING/MONITORING AGENCY NAME(S) AND ADDRESS(ES) | 10. SPONSOR/MONITOR'S ACRONYM(S) |
| | 11. SPONSOR/MONITOR'S REPORT NUMBER(S) |

12. DISTRIBUTION/AVAILABILITY STATEMENT

**Approved for public release; distribution unlimited.**

13. SUPPLEMENTARY NOTES

14. ABSTRACT

**This final report documents the research work conducted in the previous one year for the project ?Design of Tunable, Thin and Wide-band Microwave Absorbers?. It consists of two major parts: the first part (Section 2) is the theoretical analysis of scattering by a twodimensional periodic array of vertical microstrip lines; the other (Section 3) is the design of a tunable microwave absorber. Simulated results are also provided to demonstrate the two operating states of the designed tunable absorber. The final section summarizes the further work to be conducted in the next one year.**

15. SUBJECT TERMS

| 16. SECURITY CLASSIFICATION OF: | | | 17. LIMITATION OF ABSTRACT | 18. NUMBER OF PAGES | 19a. NAME OF RESPONSIBLE PERSON |
|---|---|---|---|---|---|
| a. REPORT | b. ABSTRACT | c. THIS PAGE | | | |
| **unclassified** | **unclassified** | **unclassified** | | **14** | |

# 1. Introduction

This final report documents the research work conducted in the previous one year for the project "Design of Tunable, Thin and Wide-band Microwave Absorbers". It consists of two major parts: the first part (Section 2) is the theoretical analysis of scattering by a two-dimensional periodic array of vertical microstrip lines; the other (Section 3) is the design of a tunable microwave absorber. Simulated results are also provided to demonstrate the two operating states of the designed tunable absorber. The final section summarizes the further work to be conducted in the next one year.

# 2. Scattering by a 2D Periodic Array of Vertical Microstrip Lines

This section provides a theoretical analysis of scattering by a two-dimensional (2D) periodic array of vertical microstrip lines. Section 2.1 studies the propagation characteristics of a 2D array of vertically placed microstrip lines. Section 2.2 solves the air-to-microstrip line discontinuity using Floquet modes in the air region. Numerical results for the scattering characteristics of the air-to-array discontinuity are also presented.

## 2.1 Propagation Characteristics

Figure 1 shows a 2-D periodic array of vertically placed microstrip lines. It is seen that the unit-cell of this array is basically a microstrip line sandwiched between two periodic boundaries. Under an oblique incidence, the periodic boundary can be characterized by a phase shift $\Phi_x$, which is a function of the angle of incidence. The top and bottom PEC planes refer to the ground of a printed circuit board. Since the problem of a 2-D array can be reduced to that of a unit-cell based on Floquet theorem [1], we can therefore study the propagation characteristics of the unit-cell using an efficient full-wave mode-matching method.

The unit-cell can be divided into three distinct regions, as shown in Fig. 1(c). Region I consists of an inhomogeneous waveguide that supports LSE and LSM modes [1]. This inhomogeneous region is further divided into two sub-regions (i), (ii). We use the following $y$-directed Hertzian potentials:

$$\begin{aligned}\phi^{Ih} &= e^{-j\beta z}\sum_{n=1}^{N_I}\left[A_n^{Ih}\frac{\sin\left\{k_{xn}^{Ih}(x-x_1)\right\}}{\sin\left(k_{xn}^{Ih}x_1\right)}+B_n^{Ih}\frac{\cos\left\{k_{xn}^{Ih}(x-x_1)\right\}}{\cos\left(k_{xn}^{Ih}x_1\right)}\right]F_{yn}^{Ih},\\ \phi^{Ie} &= e^{-j\beta z}\sum_{n=1}^{N_I}\left[A_n^{Ie}\frac{\cos\left\{k_{xn}^{Ie}(x-x_1)\right\}}{\cos\left(k_{xn}^{Ie}x_1\right)}+B_n^{Ie}\frac{\sin\left\{k_{xn}^{Ie}(x-x_1)\right\}}{\sin\left(k_{xn}^{Ie}x_1\right)}\right]F_{yn}^{Ie},\end{aligned} \tag{1}$$

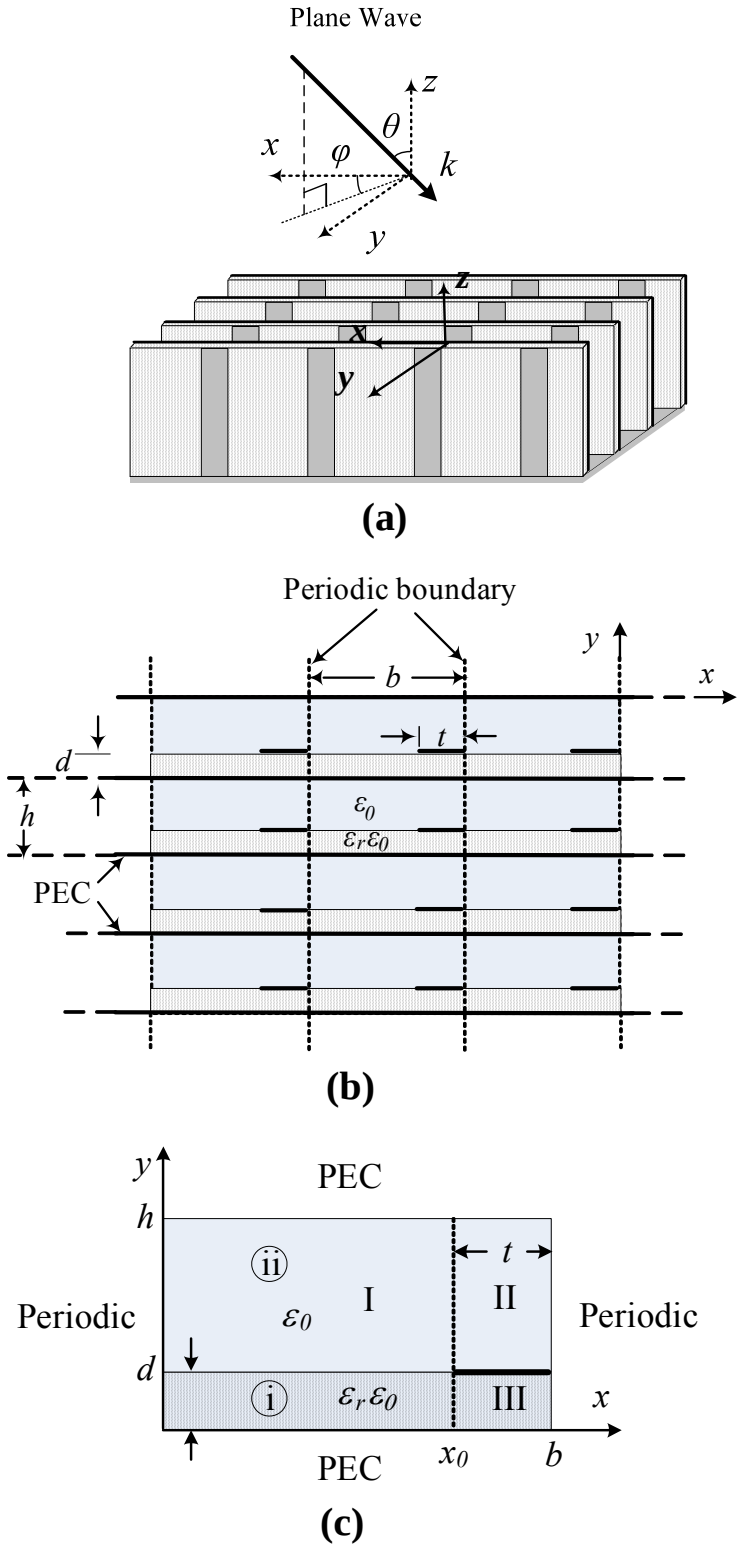


Fig. 1. Geometry of a 2-D periodic array of vertically placed microstrip lines, (a) perspective view, (b) top view, (c) cross-sectional view of a unit-cell.

where

$$F_{yn}^{Ih}=\begin{cases}\dfrac{\sin\left(k_{yn}^{Ih(i)}y\right)}{\sin\left(k_{yn}^{Ih(i)}d\right)} \\ \dfrac{\sin\left[k_{yn}^{Ih(ii)}\left(h-y\right)\right]}{\sin\left[k_{yn}^{Ih(ii)}\left(h-d\right)\right]}\end{cases}, \quad F_{yn}^{Ie}=\begin{cases}\dfrac{\cos\left(k_{yn}^{Ie(i)}y\right)}{\varepsilon_r\cos\left(k_{yn}^{Ie(i)}d\right)} & 0<y<d \\ \dfrac{\cos\left[k_{yn}^{Ie(ii)}\left(h-y\right)\right]}{\cos\left[k_{yn}^{Ie(ii)}\left(h-d\right)\right]} & d<y<h\end{cases},$$

$$\frac{\tan\left(k_{yn}^{Ih(i)}d\right)}{k_{yn}^{Ih(i)}}+\frac{\tan\left[k_{yn}^{Ih(ii)}\left(h-d\right)\right]}{k_{yn}^{Ih(ii)}}=0,$$

$$\frac{k_{yn}^{Ie(i)}\tan\left(k_{yn}^{Ie(i)}d\right)}{\varepsilon_r}+k_{yn}^{Ie(ii)}\tan\left[k_{yn}^{Ie(ii)}\left(h-d\right)\right]=0,$$

$$k_{xn}^{Ip}=+\sqrt{\varepsilon_r k_0^2-\beta^2-\left(k_{yn}^{Ip(i)}\right)^2}, \qquad p=h,e.$$

and $$x_0=b-t, \qquad x_1=\frac{x_0}{2}.$$

Fields in Region II are also derived from their *y*-directed potentials:

$$\begin{aligned}\phi^{IIh}&=e^{-j\beta z}\sum_{n=1}^{N_{II}}F_{xn}^{IIh}\sin\left\{k_{yn}^{IIh}\left(y-d\right)\right\},\\ \phi^{IIe}&=e^{-j\beta z}\sum_{n=0}^{N_{II}-1}F_{xn}^{IIe}\cos\left\{k_{yn}^{IIe}\left(y-d\right)\right\},\end{aligned} \qquad (2)$$

where

$$F_{xn}^{IIh}=\left[A_n^{IIh}\frac{\sin\left\{k_{xn}^{IIh}\left(x-x_2\right)\right\}}{\sin\left(k_{xn}^{IIh}t/2\right)}+B_n^{IIh}\frac{\cos\left\{k_{xn}^{IIh}\left(x-x_2\right)\right\}}{\cos\left(k_{xn}^{IIh}t/2\right)}\right],$$

$$F_{xn}^{IIe}=\left[A_n^{IIe}\frac{\cos\left\{k_{xn}^{IIe}\left(x-x_2\right)\right\}}{\cos\left(k_{xn}^{IIe}t/2\right)}+B_n^{IIe}\frac{\sin\left\{k_{xn}^{IIe}\left(x-x_2\right)\right\}}{\sin\left(k_{xn}^{IIe}t/2\right)}\right],$$

$$k_{yn}^{IIp}=\frac{n\pi}{h-d}, \qquad k_{xn}^{IIp}=+\sqrt{k_0^2-\beta^2-\left(k_{yn}^{IIp}\right)^2}, \; x_2=x_0+\frac{t}{2}.$$

Expressions for Region III potentials can be obtained from (2) by replacing *'y-d'* and *'h-d'* with *y* and *d*, respectively. The following boundary conditions are enforced on the tangential field components at the regional interface and the periodic boundaries.

$$E_t^I\Big|_{x=x_0} = \begin{cases} E_t^{II}\Big|_{x=x_0} \\ E_t^{III}\Big|_{x=x_0} \end{cases}, H_t^I\Big|_{x=x_0} = \begin{cases} H_t^{II}\Big|_{x=x_0} & y > d \\ H_t^{III}\Big|_{x=x_0} & y < d \end{cases},$$

$$E_t^I\Big|_{x=0} = \begin{cases} e^{-j\Phi_x} E_t^{II}\Big|_{x=b} \\ e^{-j\Phi_x} E_t^{III}\Big|_{x=b} \end{cases}, H_t^I\Big|_{x=0} = \begin{cases} e^{-j\Phi_x} H_t^{II}\Big|_{x=b} & y > d \\ e^{-j\Phi_x} H_t^{III}\Big|_{x=b} & y < d \end{cases}.$$

where $E_t^p$ and $H_t^p$ denote the tangential electric and magnetic fields in region $p$. $\Phi_x$ is the phase shift between two adjacent periodic boundaries, which can be related to the incident angle. Solving these boundary conditions through suitable orthogonal relations leads to a system of linear equations. It is then transformed to a matrix equation whose non-trivial solution yields the propagation constant $\beta$.

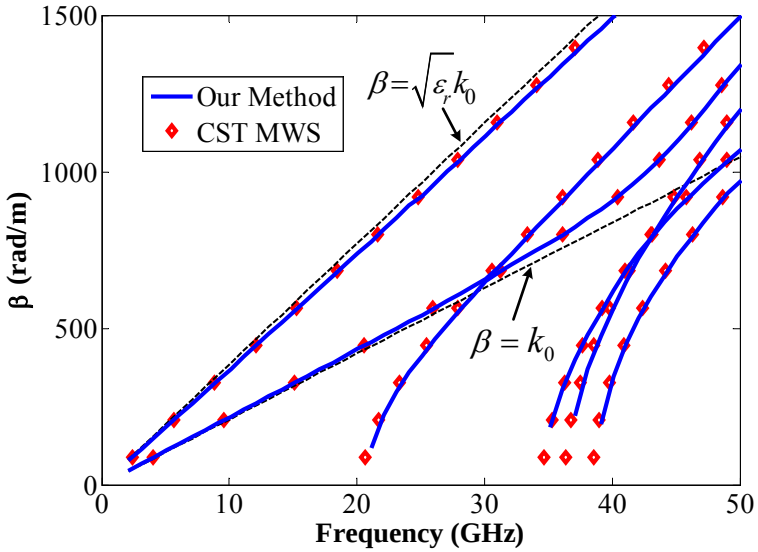


Fig. 2. Dispersion diagram of the first six modes of a periodic array of microstrip lines ($t$ = 2 $mm$, $b$ = 5 $mm$, $h$ = 5 $mm$, $d$ = 1.524 $mm$, $\varepsilon_r$ = 3.38, $\Phi_x = 0$).

Fig. 2 shows a comparison of the dispersion diagram generated by our method with the one obtained from CST Microwave Studio (MWS). An excellent agreement can be observed. Considering a small phase shift, we can observe the existence of two quasi-TEM modes. When $\Phi_x$ = 0, these two modes are similar to those of a microstrip line shielded with PMC side walls. Fig. 3 illustrates the field patterns of these two quasi-TEM modes. Most of the power carried by the first mode is concentrated in the substrate region, while the second propagates dominantly in the air region above the substrate [2].

Fig. 4 shows the variation of propagation constants of the first three modes when $\Phi_x$ is varied from 0 to 120°. In the region of lower frequencies, propagation constants of these modes decrease with an increase in the periodic phase shift. The substrate mode remains almost stable while the air-mode becomes evanescent at lower frequencies when the

periodic phase shift is increased, as shown in Fig. 4. Basically, when the periodic phase shift is $\Phi_x = 0^o$, virtual magnetic walls may be considered between the strips of the periodic array of microstrip lines. Hence, the existence of two quasi-TEM modes can be attributed to the presence of three isolated conductors in this case. On the other extreme, when $\Phi_x = 180^o$, a virtual PEC wall may be considered between the strips. Since this geometry is known to support the propagation of single quasi-TEM mode, it may explain the variation of the air-mode in Fig. 4, which becomes evanescent with an increase of the periodic boundary phase shift.

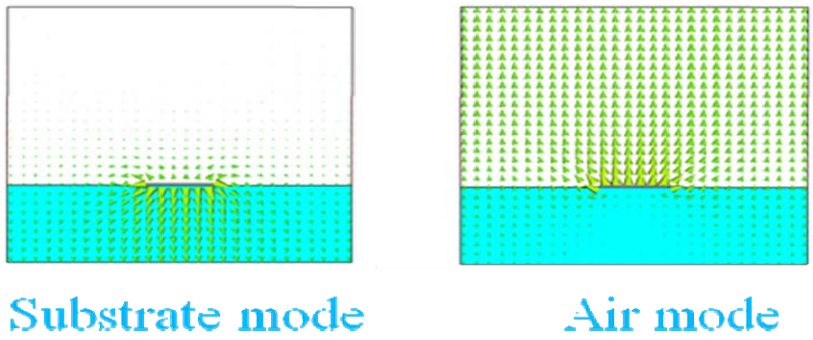


Figure 3: Field patterns of the two dominant modes in a shielded microstrip line with periodic boundaries at two side walls.

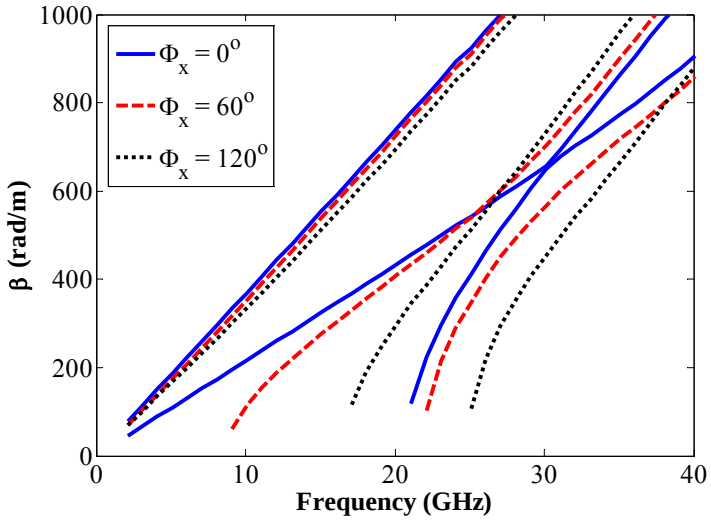


Fig. 4. Variation of the propagartion constant β as a function of periodic phase shift $\Phi_x$ for first three modes of a periodic array of microstrip lines, ($t$ = 2 *mm*, $b$ = 5 *mm*, $h$ = 5 *mm*, $d$ = 1.524 *mm*, $\varepsilon_r$ = 3.38).

## 2.2 Air-to-Array Discontinuity

Fig. 5 shows a unit-cell of the proposed array of thickness $L$, which is illuminated by a plane wave incident from air. Regions 1 and 2 denote the air region and the microstrip

line region, respectively. Based on Floquet's theorem, the problem of air-to-array discontinuity is also reduced to that of an air-to-microstrip line discontinuity.

Tangential field components in Region 1 can be written as:

$$\begin{aligned}\vec{E}_t^{(1)} &= \sum_{p=-P}^{P}\sum_{q=-Q}^{Q}\sum_{r=1}^{2}\left[C_{pqr}^{+}e^{j\beta_{pqr}^{(1)}z} + C_{pqr}^{-}e^{-j\beta_{pqr}^{(1)}z}\right]\vec{e}_{pqr}^{(1)},\\ \vec{H}_t^{(1)} &= \sum_{p=-P}^{P}\sum_{q=-Q}^{Q}\sum_{r=1}^{2}\left[C_{pqr}^{+}e^{j\beta_{pqr}^{(1)}z} - C_{pqr}^{-}e^{-j\beta_{pqr}^{(1)}z}\right]Y_{pqr}^{(1)}\left(\hat{a}_z\times\vec{e}_{pqr}^{(1)}\right),\end{aligned} \tag{3}$$

where $C_{pqr}^{+}$ and $C_{pqr}^{-}$ are the coefficients of incident and reflected waves, respectively. $\beta_{pqr}^{(1)}$ denotes the propagation constant of a mode. Expressions for transverse modal field $\vec{e}_{pqr}^{(1)}$ and admittance $Y_{pqr}^{(1)}$ are given in [3]. Region 2 supports hybrid modes as follows,

$$\begin{aligned}\vec{E}_t^{(2)} &= \sum_{n=1}^{N}\left[D_n^{+}e^{-j\beta_n^{(2)}z} + D_n^{-}e^{j\beta_n^{(2)}z}\right]\vec{e}_n^{(2)},\\ \vec{H}_t^{(2)} &= \sum_{n=1}^{N}\left[D_n^{+}e^{-j\beta_n^{(2)}z} - D_n^{-}e^{j\beta_n^{(2)}z}\right]\vec{h}_n^{(2)},\end{aligned} \tag{4}$$

where $D_n^{+}$ and $D_n^{-}$ are the coefficients of the forward and backward waves, respectively. Expressions of the transverse modal fields $\vec{e}_n^{(2)}$, $\vec{h}_n^{(2)}$ are derived from the previous section. Modal fields in the two regions are normalized according to the following orthogonality relations [3]:

$$\int_0^h\int_0^b \vec{e}_r^{(1)}\cdot\vec{e}_s^{(1)*}dxdy = 0, \qquad \int_0^h\int_0^b \vec{e}_r^{(2)*}\times\vec{h}_s^{(2)}dxdy = 0, \quad r\neq s.$$

Enforcing the continuity of tangential field components at the air-to-microstrip line interface $z = 0$ results in two sets of equations:

$$\left[C_u^{+} + C_u^{-}\right] = \sum_{n=1}^{N}\left[D_n^{+} + D_n^{-}\right]G_{un}, \tag{5a}$$

$$\sum_{s=1}^{S}\left[C_s^{+} - C_s^{-}\right]Y_s^{(1)}\bar{G}_{us} = \left[D_u^{+} - D_u^{-}\right], \tag{5b}$$

where '$s$' is a unified index for '$pqr$' modes in Region 1, and

$$G_{un} = G(u,n) = \int_0^b\int_0^h\left(\vec{e}_u^{(1)*}\cdot\vec{e}_n^{(2)}\right)dxdy, \quad \bar{G}_{us} = \int_0^b\int_0^h\left(\vec{e}_u^{(2)*}\cdot\vec{e}_s^{(1)}\right)dxdy.$$

The generalized scattering matrix of the air-to-array discontinuity is calculated as:

$$\begin{bmatrix} \mathbf{S}_{11}^s & \mathbf{S}_{12}^s \\ \mathbf{S}_{21}^s & \mathbf{S}_{22}^s \end{bmatrix} = \begin{bmatrix} \mathbf{I}^{(1)} & -\mathbf{G} \\ -\mathbf{Y}^{(1)}\bar{\mathbf{G}} & \mathbf{I}^{(2)} \end{bmatrix}^{-1} \begin{bmatrix} -\mathbf{I}^{(1)} & \mathbf{G} \\ -\mathbf{Y}^{(1)}\bar{\mathbf{G}} & \mathbf{I}^{(2)} \end{bmatrix}, \tag{6}$$

where $\mathbf{I}^{(1)}$ and $\mathbf{I}^{(2)}$ are the identity matrices of sizes $S$ x $S$ and $N$ x $N$, respectively.

An array of finite thickness can be modeled as a cascaded junction of two air-to-array discontinuities, and its S-parameters can be easily calculated [3].

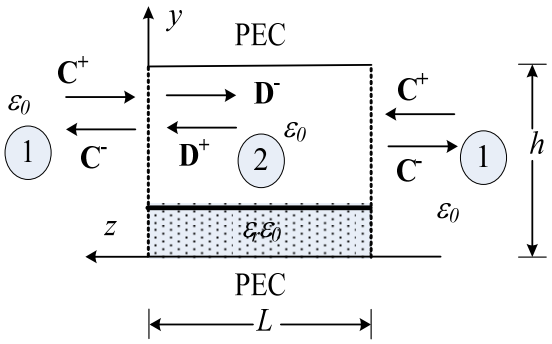


Fig. 5. Cross-sectional view of the unit-cell of a finite length array illustrating a cascaded junction of two air-to-microstrip line discontinuities.

For the given angles of incidence $\theta$ and $\varphi$, we first express the periodic boundary shift as $\Phi_x = -(k_0 \sin\theta\cos\varphi)b$, calculate the modes of Region 2, and then apply the above procedure to obtain scattering parameters.

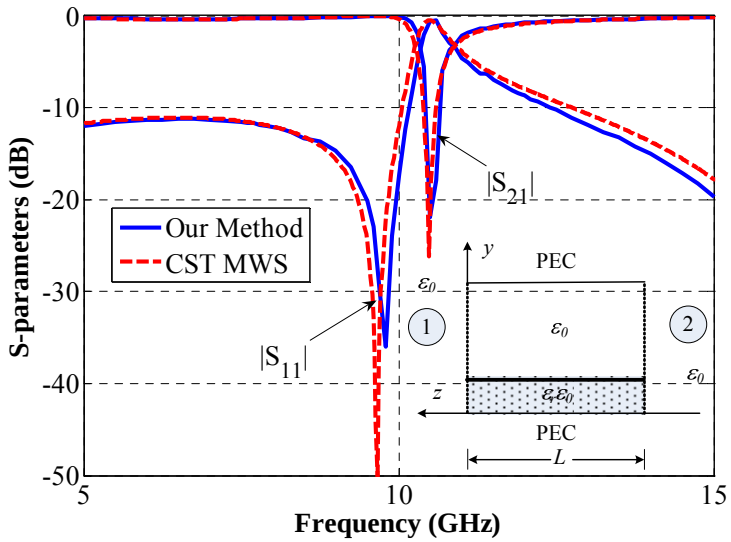


Fig. 6. S-parameters of a cascaded junction of two air-to-array discontinuities under TE incidence ($t$ = 0.2 *mm*, $b$ = 5 *mm*, $h$ = 3.124 *mm*, $d$ = 1.524 *mm*, $\varepsilon_r$ = 3, $L$ = 9.5 *mm*, $\varphi$ = 0, $\theta$ = 40°).

Fig. 6 compares our results with those obtained from CST MWS, whereby a very good agreement is noted. Fig. 7 shows the reflection coefficient of a single air-to-array discontinuity for $TE_{00}$ and $TM_{00}$ Floquet modes. It also presents the transmission coefficients of the first two modes of the microstrip line region, where $S_{21}(1)$ and $S_{21}(2)$ refer to the substrate-mode and the air-mode, respectively. It may be noted that most of the incident energy carried by $TE_{00}$ Floquet mode is coupled to the air-mode (second mode) of microstrip lines. This is understandable from the field distribution of the air-mode shown in Fig. 3. On the other hand, the first two modes of the array are not excited by the $TM_{00}$ Floquet mode. Therefore, it results in strong reflection, as seen in Fig. 7 (b).

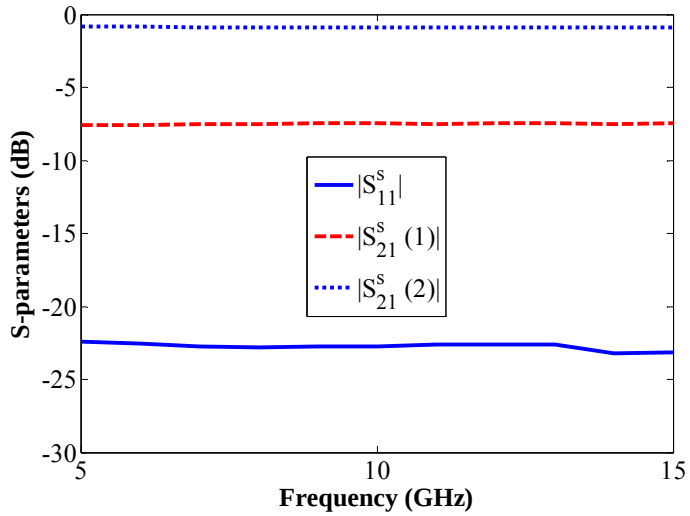


(a) TE incidence

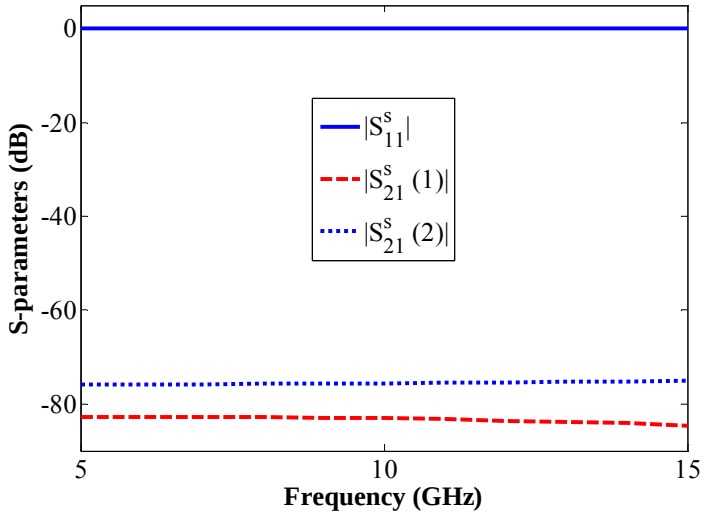


(b) TM incidence

Fig. 7. Reflection coefficient of air-to-microstrip line discontinuity, and transmission coefficients of the first two propagating modes under TE and TM indidence ($t$ = 2 *mm*, $b$ = 5 *mm*, $h$ = 5 *mm*, $d$ = 1.524 *mm*, $\varepsilon_r$ = 3.38 , $\varphi$ = 0, $\theta$ = 0).

# 3. Design of Tunable Absorber

After a careful study of the scattering characteristics of a two-dimensional periodic array of vertically placed microstrip lines described in the previous section, we designed a wide-band circuit analog absorber [4] based on the broad-band matching of free space to a short-circuited transmission line [5]. During the past one year, researchers at Nanyang Technological University (NTU), Singapore, together with Prof. Raj Mittra of Penn State University, have conducted the following work for the project (AOARD-10-1-4061) to design a tunable, thin and wide-band microwave absorber.

(i) A new study of the absorption by employing lumped circuit elements in the printed transmission lines has been conducted to achieve a thin and wide-band absorbing structure. It is found that for a unit cell, a series connection of lumped resistor $R$ and capacitance $C$ together with a parasitic inductance in the connecting line can produce an improved wide absorption bandwidth, as shown in Fig. 8 [6].

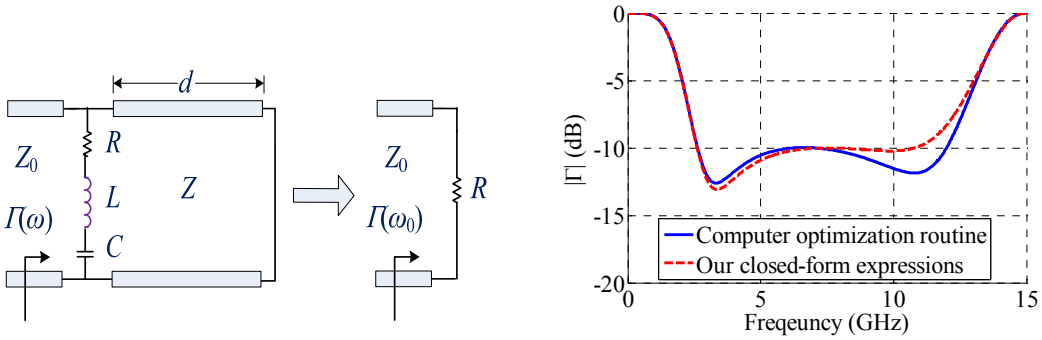


Fig. 8. Equivalent circuit model and simulated results of a broad-band matching to a short-circuited transmission using shunt RLC .

(ii) By inserting PIN diodes in the printed transmission lines a design of tunable microwave absorber has been obtained. By changing the biasing voltage across the PIN diode, it can serve either short-circuit ('ON' state) or open-circuit ('OFF' state), which produces two states for the tunable absorber. Simulated results show that the first state achieves a frequency range from 2GHz to 5.8GHz and the second state covers from 5.5GHz to 9GHz. Fig. 9 shows the geometry of the tunable microwave absorbing structure. Simulated absorbing performance of the structure under two states for both normal and oblique incidences is illustrated in Fig. 10 and Fig. 11. The design model has been finalized and is currently under fabrication. Due to delays in shipping the dielectric substrates and a mistake in fabricating one board, measured results are not available at the moment. Measured results of its absorbing

performance and tuning range will be provided and compared with our simulated results in the near future.

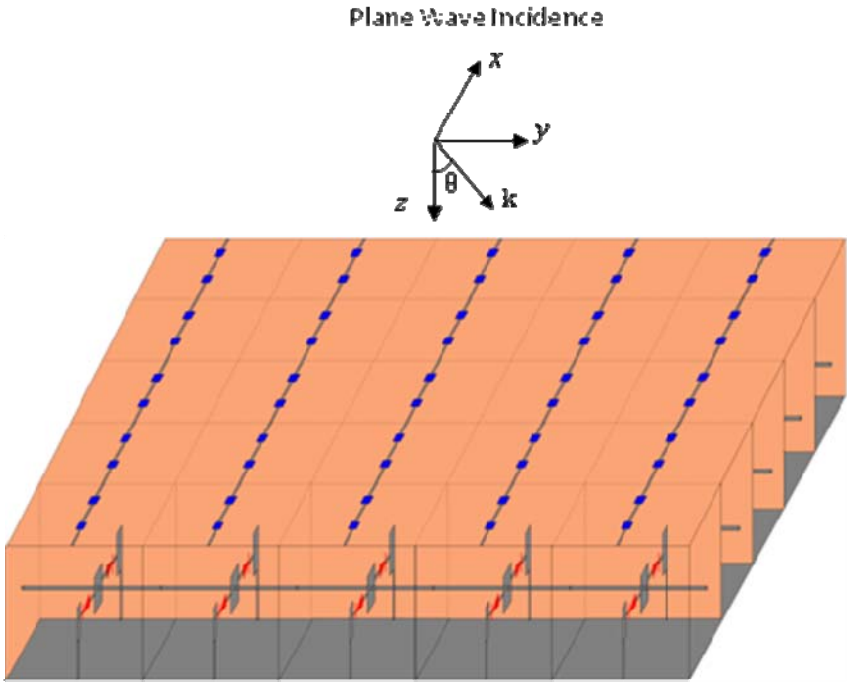


Fig. 9. Geometry of the designed tunable microwave structure with lumped circuit elements and DC biasing circuits.

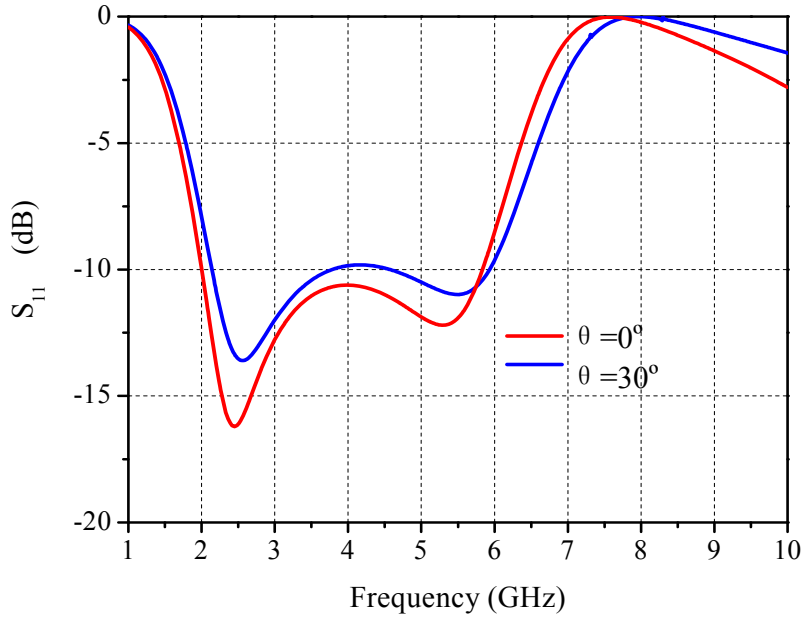


Fig. 10. Simulated results of the absorbing structure under State 1 (pin diodes are reverse-biased).

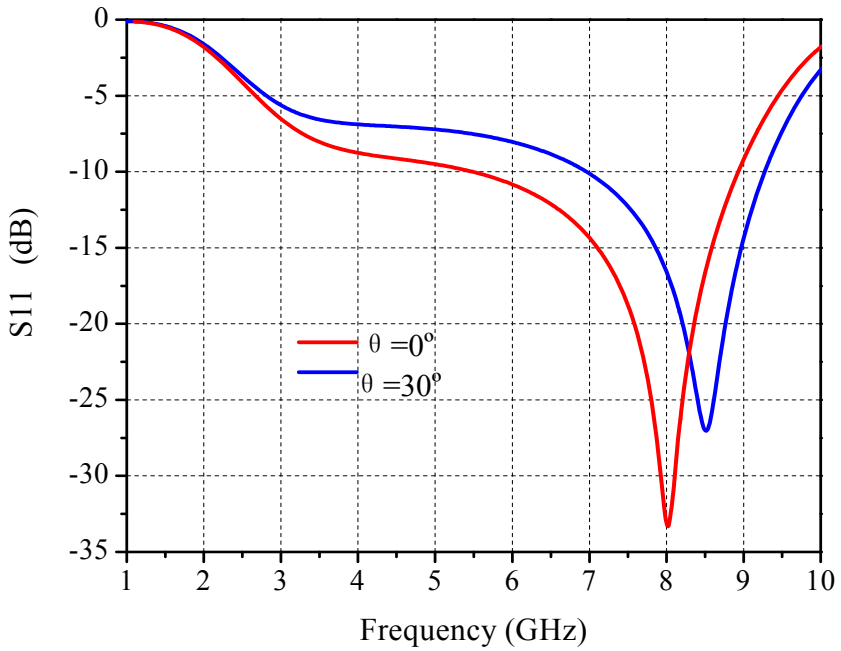


Fig. 11. Simulated results of the absorbing structure under State 2 (pin diodes are forward-biased).

# 4. Recommendations for Further Work

Based on the investigations conducted in the previous year, we envisage that there are still a number of issues to be addressed for the proposed tunable absorber.

(a) The thickness of our designed tunable absorber may be improved. Although the current thickness is already very thin (less than one-tenth free-space wavelength at the lowest frequency), there is still room for improvement. It is known that one effective way to substantially reduce the thickness of a microwave absorber is to incorporate a very thin layer of magnetic material. A careful study may be carried out to look into how to insert a very thin layer of magnetic material into our structure to significantly reduce the absorber thickness.

(b) It is seen that the bandwidth of our designed absorber may also be improved, especially for the second state (high frequency band). A new concept proposed by Prof. Mittra during his recent visit to NTU is to employ wide-band array antenna structures to broaden the bandwidth of microwave absorbers. Wide-band array antennas are excellent wide-band transitions between free space and guided transmission lines and they may effectively enhance the absorption bandwidth of our absorbing structure. An investigation into the combination of wide-band antenna structure and microwave absorber is worthwhile and may produce unexpected results.

(c) It is noted that our designed tunable absorber operates under a linear polarization when the electric field is pointing in the direction normal to the microstrip line. It is not an effective absorber under other polarizations. It would be much more useful and practical if our absorber could operate under dual polarizations. A change in the absorbing structure will be necessary to make the unit cell as symmetric along both axes as possible, which will produce an absorber for incident waves of arbitrary polarization.

In view of the mentioned issues associated with our proposed microwave absorber, we intend to continue our investigations into the design of tunable, thin and wideband microwave absorbers in the following one year. More specifically, we intend to address the three key issues raised above.

(1) A careful study will be conducted to reduce the thickness of our absorbing structure by inserting a very thin layer of magnetic material. Existing and available magnetic materials will be studied for our purpose and a demonstration will be provided to show the effect on the absorber thickness by incorporating the thin layer of magnetic material.
(2) The concept of combining wide-band array antennas with our proposed absorbing structure will be thoroughly investigated to potentially widen the bandwidth of the designed absorber. With the wide-band array antenna, the incident plane wave can be more smoothly and effectively coupled to the guided mode traveling along the transmission line, which may significantly widen the absorption bandwidth of our tunable absorber.
(3) If a square unit cell can be used, one may expect to achieve a dual-polarized microwave absorber, which should be more useful in practice. It is hoped that several possible structures can be investigated in the following one year to identify one promising candidate for designing dual-polarized tunable absorber.

Just like the previous one year, most of the research work will be conducted in Nanyang Technological University, Singapore, with regular email exchanges between researchers in NTU and Prof. Mittra of Penn State University. A couple of visits to NTU by Prof. Mittra may also be planned so that extensive discussions about technical details can take place. It is expected that the conducted research may result in a few journal or conference publications in the next year.

# REFERENCES


[1] R. E. Collin, *Field Theory of Guided Waves*. McGraw Hill Book Company Inc., 1960.
[2] A. K. Rashid and Z. Shen, “Scattering by a two-dimensional period array of vertically placed microstrip lines,” *IEEE Trans. on Antennas and Propagation,* vol.59, 2011.
[3] A. S. Omar and K. Schunemann, "Transmission matrix representation of finline discontinuities," *IEEE Trans. on Microwave Theory and Tech.,* vol. MTT-33, pp. 765-770, 1985.

[4] A. K. Rashid, Z. Shen, and S. Aditya, “Wideband microwave absorber based on a two-dimensional periodic array of microstrip lines,” *IEEE Trans. on Antennas and Propagation*, vol. AP-58, no.12, pp.3913-3922, Dec. 2010.
[5] Z. Shen and H. Wang, "On the optimum design of a thin absorbing screen," *IEEE Antennas and Propagation Society International Symposium,* pp. 6039-6042, 2007.
[6] A. K. Rashid, Z. Shen, and R. Mittra, “On the optimum design of a single-layer thin wideband radar absorber,” IEEE AP-S International Symposium, Spokane, 2011.